Available online at www.sciencedirect.com
ScienceDirect
Carbohydrate Research 343 (2008) 328–340
Carbohydrate RESEARCH

Effect of pH on the association behavior in aqueous solutions of pig gastric mucin

Atoosa Maleki,[a] Géraldine Lafitte,[b] Anna-Lena Kjøniksen,[a] Krister Thuresson[b,c] and Bo Nyström[a,*]

[a]*Department of Chemistry, University of Oslo, PO Box 1033, Blindern, N-0315 Oslo, Norway*
[b]*Physical Chemistry 1, Center for Chemistry and Chemical Engineering, Lund University, PO Box 124, SE-221 00 Lund, Sweden*
[c]*Camurus AB, Ideon Science Park, SE-223 70 Lund, Sweden*

Received 20 August 2007; received in revised form 9 October 2007; accepted 9 October 2007
Available online 13 October 2007

Abstract—In this study, dynamic light scattering (DLS), turbidity, and rheo-small angle light scattering (rheo-SALS) methods have been utilized to examine the impact of pH ($1 \leqslant pH \leqslant 7$) on aqueous solutions of noncommercial purified pig gastric mucin. The asymmetric flow field-flow fractionation (AFFFF) measurements established that the mucin sample has a high molecular weight and is polydisperse. DLS measurements on dilute solutions of mucin disclosed large interchain aggregates at pH 2, where the polymer has a low charge density or is uncharged. At lower or higher values of pH, mucin is charged and the tendency of forming interpolymer complexes is affected. In the semidilute concentration regime, pronounced junction zones ('lumps' of polymer) are evolved and a heterogeneous connected network is formed at pH 2, whereas the association structures are disintegrated (smaller 'lumps') at lower or higher pH values due to electrostatic repulsive interactions, and a more homogeneous network is evolved. The DLS and viscosity results at pH 1 indicate the development of a fragmented network, composed of contracted chains that are decorated by some positive charges. The effect of shear flow on the structure of semidilute solutions of mucin was investigated with the aid of rheo-SALS methods. The scattered intensity revealed a strong upturn at low values of the wave vector (q) for mucin solutions at pH 2 and pH 4, which suggests the evolution of large association domains. At these pH values, a flow-induced anisotropy in the 2D SALS patterns in the form of elliptical shapes was observed at high shear rates.

Keywords: Purified pig gastric mucin; Dynamic light scattering; Rheo-small angle light scattering; Effect of pH; Associations

1. Introduction

Mucins are high molecular weight ($>10^6$) polymeric glycoproteins with broad molecular weight distribution and they are components of the slimy mucus secretion that covers epithelial cell surfaces.[1,2] Mucins are primarily responsible for the protective effect of the viscoelastic mucous barrier.[3] The protective function of this layer is especially critical in the stomach during active digestion, where the pH of the gastric lumen is between 1 and 2, whereas the epithelial surface has typically a pH around 7.[1] In light of this, a fundamental understanding of the effect of pH on the mucin–mucin interactions is an important issue.

The mucin molecules consist of a linear polypeptide backbone and radially arranged oligosaccharide chains (70–80 wt %),[4] and the glycosylated domains are enriched with serine or threonine, which are linked to oligosaccharides via bonding with *N*-acetylglucosamine, *N*-acetylgalactosamine.[2,3,5] The unglycosylated areas, which normally exist with both *N*- and *C*-terminal ends, contain a large number of cysteine-rich domains and charged amino acids.[2,3,5] The electrostatic character of mucin is governed by charges both within the polypeptide backbone, for example, glutamic acid and aspartic acid residues ($pK_a \approx 4$)[6] as well as in the oligosaccharide side chains, for example, sialic acid residues ($pK_a \approx 2.6$)

* Corresponding author. E-mail: bo.nystrom@kjemi.uio.no

0008-6215/$ - see front matter © 2007 Elsevier Ltd. All rights reserved.
doi:10.1016/j.carres.2007.10.005

and sulfate groups ($pK_a \approx 1$).[7] The properties of mucin in aqueous solution are mainly directed by an intricate interplay between repulsive electrostatic forces and associating hydrophobic microdomains. The negative charges are generated through the amino acids, whereas the hydrophobic microdomains along the polymer backbone largely arise from the cysteine-rich areas that is, the unglycosylated regions. From this it is evident that changes in pH will affect ionization of the sialic acid and amino acids in the peptide backbone of the mucin, making the mucin molecules negatively charged[8] above that pH and the mucin charge density increases with increasing pH. By using experimental techniques such as atomic force microscopy,[9] dynamic light scattering,[6,10] hydrophobic dye binding,[6] and pulsed field gradient-nuclear magnetic resonance,[11] it has been established that pH plays a vital role in the mucin–mucin interactions that lead to association and gelation of mucin. However, there is a lack of studies that systematically address the structural, dynamical and rheological behaviors of mucin over a wide pH range. Furthermore, a deeper understanding of the intriguing interplay between electrostatic interactions and hydrophobic association effects is needed.

In the present work, we have carried out dynamic light scattering (DLS) on both a dilute and a semidilute aqueous solution of purified pig gastric mucin, and turbidity and rheo-small angle light scattering (rheo-SALS) experiments on the semidilute sample in the pH interval from 1 to 7. By employing rheo-SALS methods, structural changes of a sample exposed to, for example, a constant shear rate can be monitored continuously during a run. By using turbidity, DLS, and rheo-SALS, pH-induced alterations of thermodynamic, dynamical, structural, and rheological properties of mucin can be probed in a systematic way. In this investigation, as well as in a previous one,[11] noncommercial purified pig gastric mucin was used. Although these freshly purified mucins are expected to introduce greater inter-batch variability than commercial ones, they are more comparable to those in the native secretion. Commercial mucin preparations have been utilized in many earlier studies because of low inter-batch variability, allowing better comparisons between polymers. However, such mucins were reported[12] to be unable to produce rheological properties comparable to those of the native mucus layer.

The aim of this work is to gain detailed insight into structural and dynamical features of mucin in the semidilute concentration regime (1 wt %) as the pH of the sample is changed. To assist in the interpretation of the findings obtained for the transient network formed in the semidilute concentration regime at different values of pH, DLS measurements were also conducted on a dilute mucin solution (0.01 wt %) to survey the behavior of individual mucin molecules.

2. Experimental

2.1. Materials

The chemicals, H_3PO_4 (phosphoric acid), NaN_3 (sodium azide), NaH_2PO_4 (sodium phosphate, monobasic), and Na_2HPO_4 (sodium phosphate, dibasic), were all purchased from Sigma–Aldrich Norway AS. Guanidinium chloride (practical grade) was obtained from Fluka. This chemical was purified before use by treating 8 M stock solutions with active charcoal followed by filtration through a PM10-Amicon® filter. Ethylenediaminetetraacetic acid (EDTA; BDH Chemicals) was used as received, as were phenylmethylsulfonylfluoride (PMSF; Sigma–Aldrich), *N*-ethylmaleimide (NEM; Sigma–Aldrich), cesium chloride (E. Merck). Buffered solutions at pH values of 1, 2, 4, and 7 were utilized in this work.

2.2. Preparation of pig gastric mucin

Stomachs from recently slaughtered pigs were used and the mucosal surface was gently rinsed with fresh tap water to remove debris from the inner surface. A detailed description of the purification procedure has been reported elsewhere.[11] Only a brief summary of the preparation of the mucin samples is given below. The mucus was collected in an extraction buffer (10 mM NaH_2PO_4, 5 mM EDTA, 6 M guanidinium chloride, pH 6.5) in the presence of proteinase inhibitors (0.1 mM PMSF and 5 mM NEM) after gently scraping the surface of the corpus region of stomachs of freshly slaughtered pigs. The presence of proteinase inhibitors in the buffer hinders the degradation of the mucin molecules.[13] The purification of the mucin samples involved exhaustive dialysis, high-speed centrifugation, and isopycnic density-gradient centrifugation. In the last step, the different biological molecules are separated according to the density. The fractions containing mucin are collected after measuring the density, the absorbance at 280 nm, and the response to the colorimetric assay based on the Periodic Acid/Schiff stain60. Indeed, only the fractions having a density between 1.41 and 1.39 g/mL, a high absorbance, and a positive response to the colorimetric assay contained mucin. The mucin samples are stored in the fridge at 4 °C before conducting all the experiments at 25 °C.

2.3. Asymmetric flow field-flow fractionation

The AFFFF experiments were conducted on an AF2000 FOCUS system (Postnova Analytics, Landsberg, Germany) equipped with an RI detector (PN3140, Postnova) and a multiangle (7 detectors in the range 35–145°) light scattering detector (PN3070, $\lambda = 635$ nm, Postnova). The mucin sample (0.3 wt % in 0.01 M NaCl, pH $\approx$ 7) was measured using a 250 μm spacer, a regenerated cellulose membrane with a cut-off of 10,000

(Z-MEM-AQU-427 N, Postnova), and an injection volume of 20 μL. The measurements were performed by employing a constant detector flow rate of 0.2 mL/min, and using a slot-pump flow rate of 0.8 mL/min. The focusing time was 6 min at a cross-flow of 4 mL/min. Thereafter, the cross-flow was reduced exponentially (exponent of 0.3) to 1.0 mL/min during a 5 min period. The cross-flow was then linearly reduced to 0.1 mL/min during a period of 5 min, and finally linearly reduced to zero for the period of 20 min.

Processing of the measured data was achieved by the Postnova software (AF2000 Control, version 1.1.011). The molecular weight of mucin was determined in the dilute concentration regime by using this software with a random coil fit, and a refractive index increment (dn/dc) of 0.144 (determined by using the RI-detector at 32 °C). From the results the weight-average molecular weight of the sample was estimated to be $M_w \approx 1.5 \times 10^7$, and the polymer has a broad molecular weight distribution ($M_w/M_n \approx 3$). Figure 1 shows a fractogram of a dilute solution of purified pig gastric mucin. This molecular weight is much higher than usually observed for commercial mucin samples, where degradation of the mucin chains during the purification process leads to a reduced molecular weight.[12]

2.4. Turbidimetry

The transmittances of 1.0 wt % solutions of mucin at different values of pH were measured with a temperature controlled Helios Gamma (Thermo Spectronic, Cambridge, UK) spectrophotometer at a wavelength of 500 nm. The apparatus is equipped with a temperature unit (Peltier plate) that gives a good temperature control over an extended time. The turbidity τ of the samples can be determined from the following relationship: $\tau = (-1/L)\ln(I_t/I_0)$, where L is the light path length in the cell (1 cm), I_t is the transmitted light intensity, and I_0 is the incident light intensity. The results from the spectrophotometer will be presented in terms of turbidity.

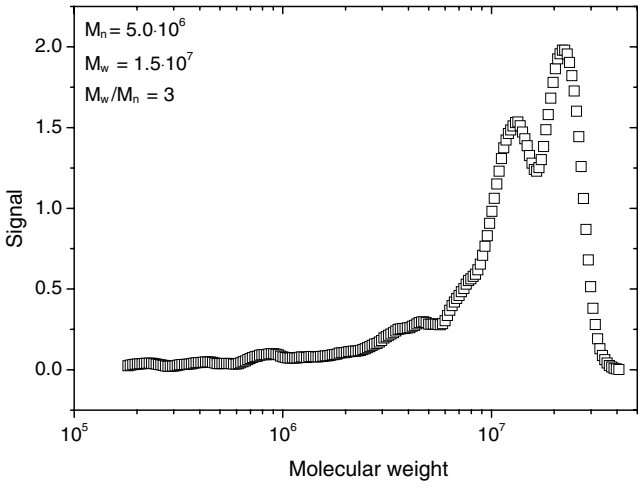

Figure 1. Fractogram of a dilute solution of purified pig gastric mucin. The data show that the molecular weight of the sample is high ($M_w = 1.5 \times 10^7$) with a fairly high polydispersity ($M_w/M_n \approx 3$).

2.5. Dynamic light scattering measurements

The setup for the intensity and dynamic light scattering experiments is an ALV/CGS-8F multi-detector version compact goniometer system, with eight off fiber-optical detection units, from ALV-GmbH, Langen, Germany. The light source is a Uniphase cylindrical 22 mW HeNe-laser, operating at a wavelength of 632.8 nm, with vertically polarized light. The beam was focused on the sample cell (10-mm NMR tubes, Wilmad Glass Co., of highest quality) through a temperature-controlled cylindrical quartz container (with two plane-parallel windows), vat (the temperature constancy being controlled to within ±0.01 °C with a heating/cooling circulator), which is filled with a refractive index matching liquid (*cis*-decalin).

The light-scattering process defines a wave vector $q = (4\pi n/\lambda)\sin(\theta/2)$, where λ is the wavelength of the incident light in a vacuum, θ is the scattering angle, and n is the refractive index of the medium. The refractive index (at 25 °C) was measured with an automatic refractometer (model PTR 46) purchased from Index Instruments Ltd, England. The temperature of the instrument is controlled electronically to a high stability by using a Peltier cell.

The full homodyne intensity autocorrelation function was measured at eight scattering angles simultaneously in the range 22–141° with four ALV 5000/E multiple-τ digital correlators. If the scattered field obeys Gaussian statistics, the measured correlation function $g^2(q,t)$ can be related to the theoretically amenable first-order electric field correlation function $g^1(q,t)$ by the Siegert relationship[14] $g^2(q,t) = 1 + B|g^1(q,t)|^2$, where B is usually treated as an empirical factor. No reduction of the initial amplitude of the correlation function could be detected at any measuring conditions, and no other signs of non-ergodicity were found for the samples considered in this work.

In the dilute concentration regime, the decays of the correlation functions were found to be unimodal and could be portrayed by a stretched exponential

$$g^1(t) = A\exp\lfloor -(t/\tau_e)^{\beta_f}\rfloor \quad (1)$$

where A is the amplitude of the relaxation mode, τ_e is some effective relaxation time, and β_f ($0 < \beta_f \leqslant 1$) is a measure of the width of the distribution of relaxation times. The mean relaxation time is given by

$$\tau = \frac{\tau_e}{\beta_f}\Gamma\left(\frac{1}{\beta_f}\right) \quad (1a)$$

where $\Gamma(\beta^{-1})$ is the gamma function of β^{-1}. The relaxation time τ is always q^2 dependent, which is the hallmark of a diffusive process, and the relaxation time is related to the mutual diffusion coefficient D_m ($\tau^{-1} = D_m q^2$). For dilute solutions of polymer coils, the apparent hydrodynamic radius R_h can be estimated from the mutual diffusion coefficient via the Stokes–Einstein relationship $D_m = k_B T/6\pi\eta_0 R_h$, where k_B is the Boltzmann constant, T is the temperature, and η_0 is the viscosity of the solvent.

For semidilute solutions of mucin the relaxation process is bimodal[6,15,16] and the decays of the correlation functions can, in analogy with other DLS studies[17,18] on complex systems, be described by a double stretched exponential

$$g^{(1)}(t) = A_f \exp\left[-\left(\frac{t}{\tau_{fe}}\right)^{\beta}\right] + A_s \exp\left[-\left(\frac{t}{\tau_{se}}\right)^{\gamma}\right] \quad (2)$$

with $A_f + A_s = 1$. The parameters A_f and A_s are the amplitudes for the fast and the slow relaxation modes, respectively. Analyses of the time correlation functions of the concentration fluctuations at long wavelengths in the semidilute concentration regime have shown that the first term (short-time behavior) on the right-hand side of Eq 2 is related to a cooperative diffusion coefficient D_c ($\tau_f^{-1} = D_c q^2$). The second term in Eq 2 (long-time feature) is associated with disengagement relaxation of individual chains or cluster relaxation.[19] As discussed above τ_{fe} and τ_{se} are some effective relaxation times, and β and γ measure the widths of the distributions of relaxation times. The mean relaxation times are given by

$$\tau_f \equiv \int_0^{\infty} \exp\left[-(t/\tau_{fe})^{\beta}\right] dt = (\tau_{fe}/\beta)\Gamma(1/\beta) \quad (2a)$$

$$\tau_s \equiv \int_0^{\infty} \exp\left[-(t/\tau_{se})^{\gamma}\right] dt = (\tau_{se}/\gamma)\Gamma(1/\gamma) \quad (2b)$$

In the analysis of the correlation function data, a nonlinear fitting algorithm (a modified Levenberg–Marquardt method) was utilized to best-fit values of the parameters appearing on the right-hand side of Eqs 1 and 2.

2.6. Rheo-small angle light scattering (rheo-SALS)

Combined rheological and small angle light scattering (rheo-SALS) experiments during shear flow were performed simultaneously using the Paar-Physica MCR 300 rheometer, equipped with a specially designed parallel plate–plate configuration (the diameter of the plate is 43 mm) in glass. The instrumentation for the rheo-SALS experiments was purchased from Physica-Anton Paar. In all measurements a 10 mW diode laser operating at a wavelength of 658 nm was used as the light source, and a polarizer is placed in the front of the laser and an analyzer below the sample, making both polarized (polarizer and analyzer parallel) and depolarized (polarizer and analyzer perpendicular) experiments possible. All experiments in this study were conducted using polarized light scattering. Utilizing a prism, the laser beam was deflected and passed through the sample placed between the transparent parallel plates. The distance between the plates is small (1.0 mm) so that the effect of multiple scattering is reduced when the sample becomes turbid at intermediate pH values. The light propagated along the velocity gradient direction thus probing the structure in the plane of flow and vorticity. The forward scattered light at small angles was collected on a flat translucent screen below the sample (distance between sample and screen is 12.3 cm).

The 2D scattering patterns formed on the screen were captured using a CCD camera (driver LuCam V. 3.8), which plane is parallel to that of the screen. A Lumenera (VGA) CCD camera (Lumenera Corporation, Ottawa, Canada) with a Pentax lens was utilized, and the scattered images were stored on a computer using the StreamPix (NorPix, Montreal, Quebec, Canada) application software (version 3.18.5), which enables a real-time digitalization of the images. The images were acquired via the CCD camera with an exposure time of 200 ms. Subsequently, the pictures were analyzed using the SALS-software program (version 1.1) developed by the Laboratory of Applied Rheology and Polymer Processing, Department of Chemical Engineering, Katholieke Universiteit Leuven, Leuven, Belgium. The scattering functions were recorded continuously during the run. The approximate accessible scattering wave vector (q) range is between $q = 4 \times 10^{-4}$ nm^{-1} and $q = 2 \times 10^{-3}$ nm^{-1}.

All the rheological and rheo-SALS measurements reported below are measured with an increasing shear rate, only small hysteresis effects were observed for measurements performed with decreasing shear rate.

3. Results and discussion

3.1. Dynamic light scattering

To obtain a more complete picture of the dynamics of mucin, DLS measurements on both a dilute and a semidilute polymer solution have been carried out at different values of pH. In the dilute regime (0.01 wt %), the behavior of more or less molecularly dispersed species was probed, and this can provide us with information about the dynamics of individual chains. In the semidilute regime (1 wt %), a transient network is formed and a concerted motion of polymer chains relative to the solvent governs the dynamics at short times, whereas at longer times the dominating feature is the disengagement relaxation of individual chains. At this stage, both

entanglements and hydrophobic associations will affect the relaxation process.

3.1.1. Dilute concentration regime. In Figure 2a, normalized correlation data for a dilute (0.01 wt %) mucin solution at various pH values, together with the corresponding curves fitted with the aid of Eq 1, are depicted in the form of semilogarithmic plots. It is clear that the longest relaxation time is observed around pH 2, and the relaxation time gradually decreases as the value of pH increases (Fig. 2b). At pH values above 2, mucin is negatively charged and the charge density increases progressively with rising pH, leading to more extended chains[20] due to enhanced electrostatic repulsions. At this stage, the entities are expected to be essentially molecularly dispersed ($R_h \approx 75$ nm; see the inset of Fig. 2b), which is consistent with the fact that the value of β_f rises with increasing pH (Fig. 2c). A more narrow distribution of relaxation times (the value of β_f approaches 1) is a sign of that the tendency of forming large interchain aggregates is reduced.

At pH close to 2, it has been reported[21] that the ionization of sialic acid is suppressed and the z-potential of mucin approaches zero. At this stage, the hydrophobic interactions dominate and large interchain complexes are formed ($R_h \approx 650$ nm). At lower pH (pH <2) it has been argued[22,23] that mucin becomes protonated and will bear a net positive charge. In view of this, the lower value of R_h at pH 1 (Fig. 2b) is ascribed to contraction of the interchain complexes, which are stabilized by some positive charges on the surfaces. The maximum of the reduced intensity at pH 2 (see Fig. 2d) is another indication of formation of large association complexes, and the lower reduced intensity at higher and lower values of pH is consistent with the hypothesis of reduced tendency of interpolymer aggregation.

Figure 3 shows the q dependence of the reduced intensity for 0.01 wt % solutions of mucin at various values of

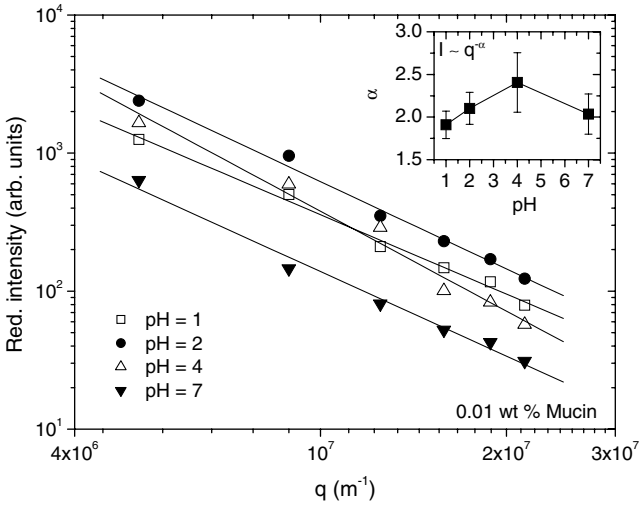

Figure 3. Log–log plot of the reduced intensity versus wave vector for 0.01 wt % solutions of mucin at various values of pH. The inset shows the effect of pH on the power law exponent α, expressing the q dependence of the intensity ($I \sim q^{-\alpha}$).

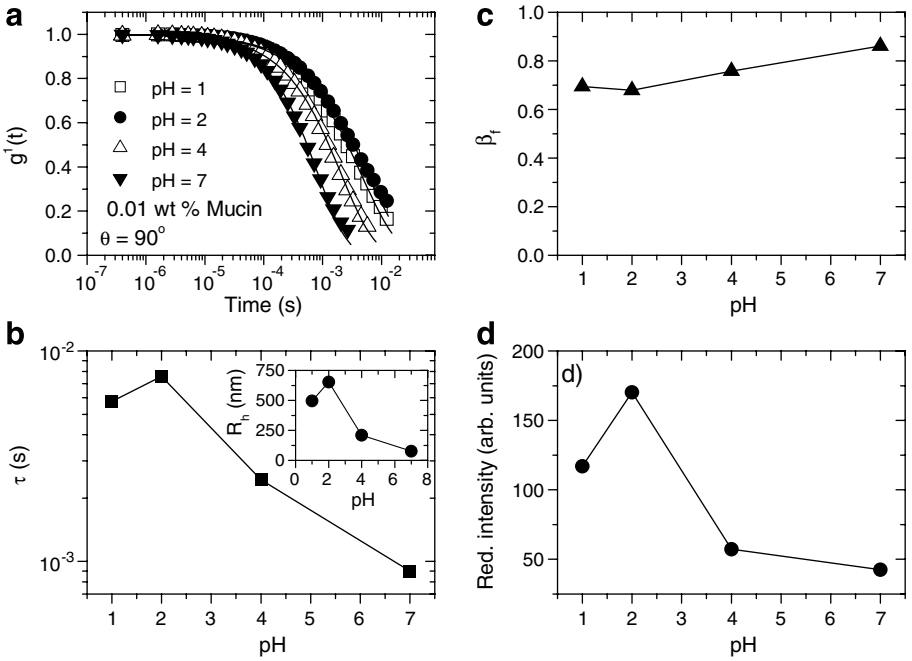

Figure 2. (a) Plot of the first order field-correlation function versus time, together with the curves fitted with the aid of Eq 1, at a scattering angle of 90° for 0.01 wt % aqueous solutions of mucin at different values of pH (every third point is shown). (b) pH dependence of the relaxation time (calculated from Eq 1a) and the inset shows the pH dependence the hydrodynamic radius (calculated from the Stokes–Einstein relationship). (c) Effect of pH on the stretched exponent β_f (see Eq 1). (d) Reduced intensity as a function of pH.

pH. In the restricted wave vector region covered in these measurements, a power law ($I(q) \sim q^{-\alpha}$) can describe the q dependence of the reduced intensity. In the 'intermediate q regime' ($qR_h > 1$), the scattering experiment probes the cluster fractal dimension[24,25] and the scattered intensity function contains information about this internal structure in the q region corresponding to the characteristic structure length. The value of α passes through a maximum at pH 4 ($\alpha = 2.4$) and at pH 1 and pH 7 the values of α are around 2, which is typical for polymer coils. The results indicate that the local structure of the species is more compact at pH 4. We may note that a similar profile of the q dependence of the reduced intensity as a function of pH is also found for the semidilute solution (see the discussion below).

3.1.2. Semidilute concentration regime. Before the results are presented and discussed, it may be instructive to give some aspects about the behavior of mucin in the semidilute concentration regime, and how the network formation is influenced by changes of pH. In a general sense, mucin can be viewed as a polyampholyte that is virtually uncharged at approximately pH 2 and with an anionic character at higher pH and cationic at lower pH (pH <2). In the semidilute concentration regime, the features of the mucin network are governed by a delicate interplay between connectivity provided by hydrophobic microdomains or 'lumps' (bundles of associating polymer chains) and swelling caused by the electrostatic repulsions. At the uncharged state of the polymer, large 'lumps' or hydrophobic association zones are formed and at a sufficiently high polymer concentration, the intensity of the interpolymer aggregation induces a macroscopic phase separation of the solution into a polymer-rich phase and an excess aqueous phase. When the value of pH rises (pH >2), the charge density of the polymer increases and the association or phase-separation behavior of mucin is modified because the repulsive forces cause fragmentation of the large domains of polymer-rich phase into microscopic 'lumps', which are stabilized by the charges on the surfaces of these 'lumps'. At pH <2 a similar picture emerges, but in this case the network is probably composed of more compressed chains that are decorated with some charges and the connectivity is weaker.

A sol–gel transition has recently been reported[26] for a concentrated high molecular weight mucin sample at pH 4. The gel formation at pH 4 can be rationalized in the scenario outlined above, which originally was developed by Cabane et al.[27] for the description of temperature-induced gelation[28] in aqueous semidilute solutions of the amphiphilic copolymer ethyl(hydroxyethyl)cellulose (EHEC) in the presence of an ionic surfactant. In this case, the surfactant is adsorbed to the polymer chains and generates repulsive forces (swelling power) while the temperature-induced hydrophobic association zones ('lumps') provide the connectivity of the network. At a certain temperature, a balance between swelling and connectivity is established and a gel network is formed. In an analogous way, we can argue that at a sufficiently high mucin concentration the required network connectivity is evolved through the hydrophobic interactions and at a certain pH (pH 4), a balance between repulsive (swelling) and attractive (connecting) forces has been established. At lower pH ($2 \leqslant \text{pH} < 4$), the 'lumps' will grow and the charge density decreases, and as a result macroscopic phase separation is approached. At higher pH (pH >4), the swelling power is enhanced and hydrophobic association zones are disrupted, leading to a situation where the permanent connectivity in the gel-network is lost and a transient network develops. Since both swelling and connectivity of the gel must be fulfilled at the same time, the incipient gel must be close to phase separation and this kinship between phase separation and gelation for physical gels has been recognized in some theoretical papers.[29–31]

In Figure 4a, normalized time correlation data for 1 wt % solutions of mucin at different values of pH, together with the corresponding curves fitted by means of Eq 2, are depicted in the form of semilogarithmic plots. A comparison of the correlation functions reveals that the long-time tail of the correlation function representing pH 2 is shifted toward the longest time. Figure 4b shows the effects of pH on the fast (τ_f) and the slow (τ_s) relaxation times for 1.0 wt % solutions of mucin. We may note that the difference in time scale between the fast and slow relaxation processes spans several orders of magnitude, and both the fast and the slow relaxation times pass through a maximum at pH 2.

In the interpretation of the results for the fast relaxation process, it should be noticed that the q dependence of the inverse fast relaxation time can be expressed as $\tau_f^{-1} \sim q^{\alpha_f}$, where α_f is, within experimental errors, at all conditions equal to 2 (see Fig. 4d), which is the hallmark for a diffusive process. In the framework of the 'blob' model for semidilute solutions,[32] the fast relaxation time ($\tau_f^{-1} = D_c q^2$) yields a cooperative diffusion coefficient that is associated with network deformation and can be defined by $D_c \approx k_B T/6\pi\eta_0\xi_h$, where ξ_h can be viewed as a characteristic mesh size of the transient network. The pH dependence of ξ_h is displayed in Figure 4c, where the screening length exhibits a maximum around pH 2. This trend may be rationalized in the following way. In view of the discussion above, large 'lumps' of mucin (bundles of associating chains) can be expected to evolve at pH 2, whereas at higher or lower values of pH the repulsive forces cause a disintegration of the 'lumps' and the chains 'loosen up'. If the correlation length ξ_h is visualized[32] as a measure of the average mesh size of the network, the observed maximum of ξ_h at pH 2 (Fig. 4c) may be associated with enhanced hydrophobic associations at this condition, giving rise

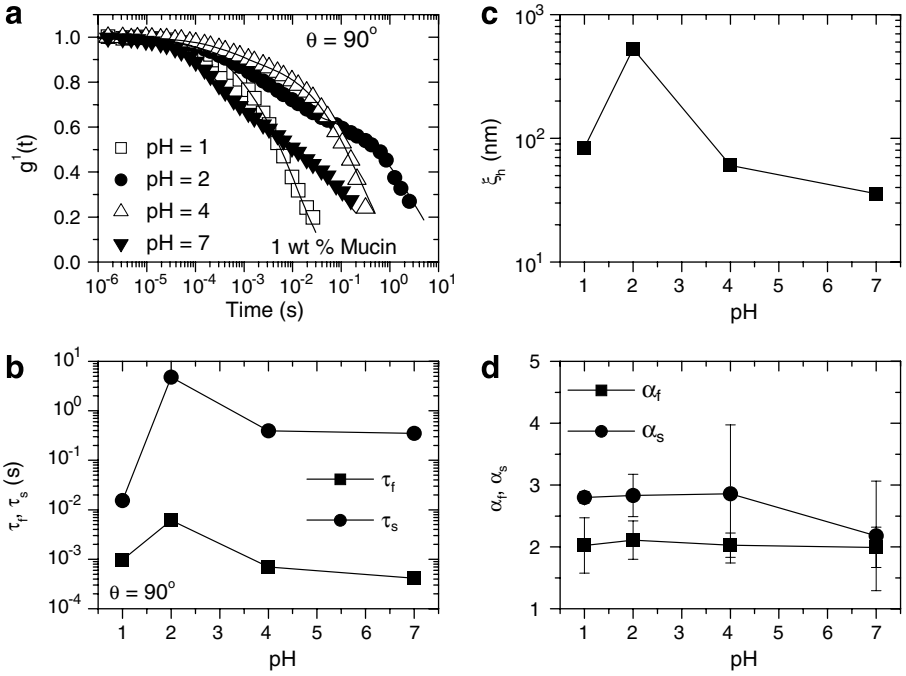

Figure 4. (a) Plot of the first order field-correlation function versus time, together with the curves fitted with the aid of Eq 2, at a scattering angle of 90° for 1.0 wt % aqueous solutions of mucin at different values of pH (every 4th point is shown). (b) pH dependences of the fast and the slow relaxation time. (c) Plot of the screening length ξ_h, calculated from the fast relaxation mode, as a function of pH. (d) Effect of pH on the power law exponents α_f and α_s, illustrating the q dependences of the fast and the slow inverse relaxation time, respectively.

to a heterogeneous network. The conjecture is that bundles of close-packed polymer chains are formed, and as a result, the effective mesh size of the network increases. At higher or lower values of pH, the charges on the chains yield a more homogeneous network structure with chains more evenly distributed in the network.

The pH dependence of the slow relaxation time (Fig. 4b) can be rationalized in the following way. In view of that the slow relaxation mode is ascribed to disengagement relaxation of individual chains or cluster relaxation, the longest relaxation time found at pH 2 is expected because at this stage the interactions between the chains should be strongest, or in terms of the coupling model of Ngai,[19] the coupling strength of the relaxation mode to its complex environments should be optimal. At lower or higher values of pH, a more loose association of chains exists because of repulsive forces and this leads to a faster relaxation. We should note that a much lower value of τ_s is detected at pH 1 than at pH 7, and this trend is consistent with the viscosity results presented below. The reason is probably that at pH 1, the network is composed of compressed chains decorated with some positive charges and the connectivity of this network with few entanglements is weak, promoting a fast relaxation of individual chains.

The wave vector dependence of the slow mode is stronger ($\alpha_s \approx 3$) than that of a diffusive process at all pH values, except at pH 7 where α_s is virtually 2 (Fig. 4d). A stronger q dependence of the slow mode is usually attributed[33–36] to internal motions of large association complexes. At pH 7, most of the large association complexes are disrupted due to the high charge density of the polymer, and this may explain the lower value of α_s at this stage. We note that since the correlation length (or mesh size) drops with increasing pH (Fig. 4c), the assumption is that the low value of α_s at pH 7 reflects crossover effects in connection with the transition from the intermediate regime $q\xi_h > 1$ to the global regime $q\xi_h < 1$, characteristic of diffusion. Actually at pH 7, essentially the global regime ($0.3 \leqslant q\xi_h \leqslant 1.4$) is probed, whereas at pH 2 the intermediate domain is monitored ($5 \leqslant q\xi_{sh} \leqslant 20$).

The effects of pH on the turbidity and the reduced intensity are displayed in Figure 5a and b, respectively. Both the turbidity and reduced intensity data curves exhibit a similar profile, with a maximum located at approximately pH 2. This supports the hypothesis that large association structures are formed at pH 2 where charge neutrality reigns, and that fragmentation of these 'lumps' occurs at lower and higher values of pH because of electrostatic interactions.

Figure 5c shows a log–log plot of the reduced intensity versus the wave vector for 1 wt % solutions of mucin at different values of pH, and the q dependence of the reduced intensity can be described by a power law $I(q) \sim q^{\alpha}$. At all pH values, except pH 4, the value of α is close to 2 (Fig. 5d) that is comparable to values of the fractal dimension reported[26,28,37,38] for solutions

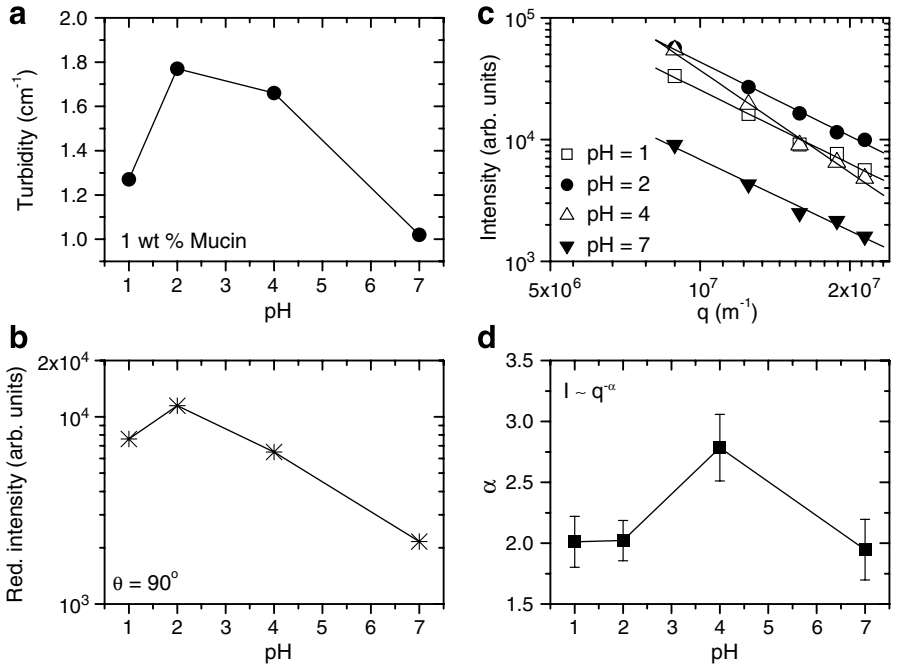

Figure 5. pH dependences of the turbidity (a) and the reduced intensity (b) for a 1 wt % solution of mucin. (c) Log–log plot of the reduced intensity versus the wave vector. (d) Effect of pH on the power law exponent α, illustrating the q dependence of the reduced intensity.

and gels of different polysaccharides. At pH 4, a fractal dimension ($\alpha \approx 2.7$) is observed that, within experimental errors, is close to the value of 2.5 predicted[39] for percolation clusters at threshold. From a recent rheological study[26] on an incipient mucin gel at pH 4, a fractal dimension of 2.1 was reported. This lower value may reflect the more pronounced entanglements at the higher polymer concentration used in that study.

3.2. Rheo-SALS

A typical correlation length and the corresponding relaxation time can characterize the dynamics and structure of a semidilute polymer solution in quiescent state, for example, the DLS results discussed above. Shear flow is expected to cause distortion of the equilibrium structure, but at low shear rates the structure is essentially preserved when the relaxation processes are fast compared to the flow velocity. In semidilute solutions of long polymer chains, reptation motion is often a dominating part of the relaxation process, and in this case the ratio of the relaxation rate and shear rate is called the Weissenberg number[40] and is used to characterize the magnitude of the shear flow. Usually, to observe an effect of shear flow on the structure it is necessary to be in the region of strong shear, that is, high Weissenberg numbers. In polymer solutions exhibiting shear thinning, a characteristic relaxation rate can be estimated from the onset of shear thinning. Figure 6a shows flow curves of 1 wt % solutions of mucin at various values of pH. All viscosity curves, except at pH 1, display a pronounced shear thinning behavior even at low shear rates. These results suggest that the relaxation process is fast at these values of pH, and the progressive decrease in viscosity as the shear rate rises indicates that the intermolecular junctions are gradually disrupted.

The most conspicuous feature in Figure 6a is the very low viscosity and practically Newtonian behavior at pH 1, which is consistent with the behavior reported previously.[11] This announces that the network structure is not fully developed and the connectivity is weak. This is compatible with the picture presented above, namely that a weak network is formed, composed of contracted chains decorated with some charges and the number of entanglement couplings is low. In Figure 6b, the zero-shear viscosity is plotted as a function of pH. It is obvious that the profile of the resulting curve is similar to the corresponding one in quiescent state found for the slow relaxation time from DLS (cf. Fig. 4b) measurements. The maximum is located at pH 2, which again emphasizes the strong associations evolved at this pH. These results are in good agreement with those in Ref. 11, considering that pH 2 was not investigated in that paper.

To examine possible structural alterations under the influence of shear flow, small angle light scattering measurements were conducted and monitored during the shear viscosity experiments. Typical SALS patterns obtained from 1 wt % solutions of mucin at different values of pH and shear rates are depicted in Figure 7. The patterns reveal that the 2D scattered intensity profile is strongest at pH 2 and pH 4. This finding indicates that multichain structures are evolved at these pH values. At

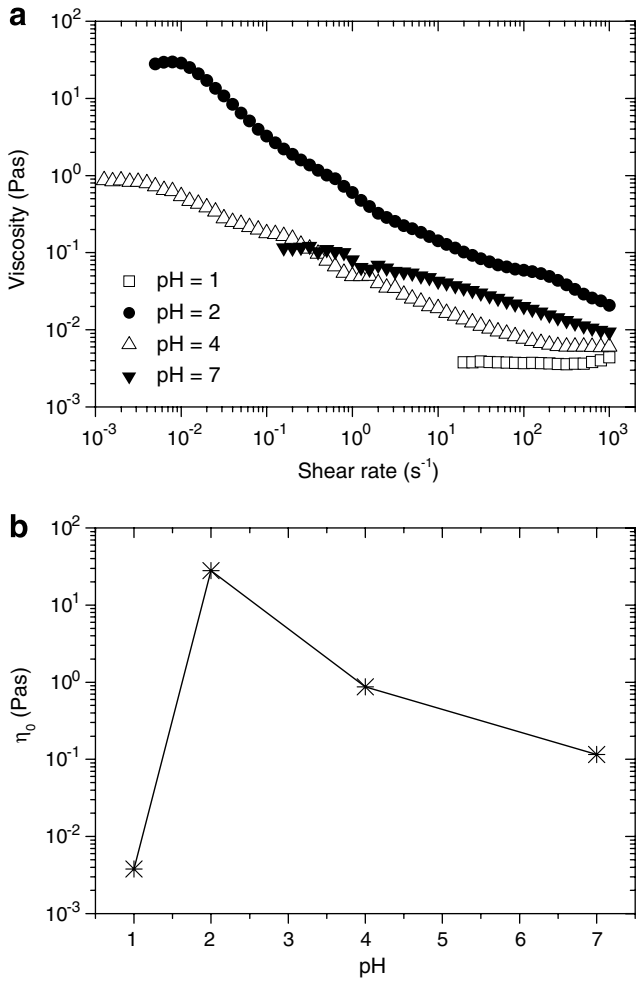

Figure 6. (a) Comparison of the shear viscosity for 1 wt % solutions of mucin at the pH values indicated. (b) Effect of pH on the zero-shear viscosity.

pH 7, weak patterns are observed at low shear rates, and augmented intensity patterns are found at high shear rates. Most of the patterns indicate that the scattered intensity is isotropic. However, at pH 2 and pH 4 at high shear rates, the scattered intensity profile shows an anisotropic pattern with an elliptical scattering pattern with a major axis parallel to the flow direction. This indicates larger amplitude of concentration fluctuations developed along the flow direction in the q range covered. These fluctuations are coupled to the applied mechanical stresses.[41–44]

Figure 8a shows the effect of shear rate on the scattered intensity at a low q-value ($q = 0.27\ \mu m^{-1}$) both along the flow direction and vertically across the flow direction in 1 wt % solutions of mucin at some different pH values. At low shear rates ($\dot{\gamma}<50\ s^{-1}$), the scattered intensity is not affected by the shear rate, and the scattered intensity in the flow direction and vertically across does not deviate significantly from each other. For the samples at pH 2 and 4, high shear rates induce anisotropy in the samples, and the scattered intensity in the flow direction is lower than what is observed vertically across. The anisotropic behavior shows that the shear forces stretches the association structures in the flow direction, and as can be seen from Figure 6, these samples also exhibit shear thinning in this regime. The sample at pH 7 is isotropic at all the measured shear rates, indicating that the weaker associations in this sample are not elongated by the shear forces. The sample at pH 1 does, however, exhibit a small tendency of anisotropy at high shear rates. For this sample, the scattered intensity in the flow direction is higher than vertically across, contrary to what is observed for the pH 2 and 4 samples. This effect can also be seen from Figure 7, where the scattering profile for the pH 1 sample at high shear rates is somewhat elongated vertically across the flow direction. From Figure 6a, it can be seen that the viscosity of this sample increases at high shear rates. This effect is probably caused by turbulence, and we believe that this turbulence is also the origin of the anisotropic behavior of this sample.

In Figure 8b, the pH dependence of the scattered intensity at a high shear rate of $500\ s^{-1}$ ($q = 0.27\ \mu m^{-1}$) along the flow direction and vertically across is depicted. The scattered intensity exhibits a broad maximum as the pH is increased, illustrating that much stronger associations develop in the pH 2 and 4 samples, compared to the samples at pH 1 and 7. This figure also shows that at this high shear rate, only the sample at pH 7 is isotropic, while the intensity along the flow direction and vertically across clearly deviates from each other for the samples at lower pH values (see the discussion above). This suggests that the concentration fluctuations become stronger when the charge density decreases.

SALS intensity profiles are displayed in Figure 9 for 1 wt % solutions of mucin at various pH values and shear rates. The open symbols illustrate the intensity values along the flow direction and the solid symbols the intensity vertically across. At low shear rates, no significant difference is observed between the scattered intensity profiles in the flow direction and vertically across, while at higher shear rates, a deviation between the scatterings in the flow direction and vertically across can be observed, especially for the pH 2 and 4 samples. The general pattern of behavior of the scattering profiles is quite similar at all studied shear rates. A salient feature is the strong upturn of the scattered intensity at low q values for mucin solutions at pH 2 and pH 4, which announces the formation of large-scale heterogeneities[45] in the solution or multichain domains.[46] This type of behavior has previously been reported from rheo-SALS[47] and small angle neutron scattering[48–50] (SANS) measurements on aqueous solutions of amphiphilic polysaccharides.

To quantitatively depict the q dependence of the scattered intensity at low q values, we have employed a

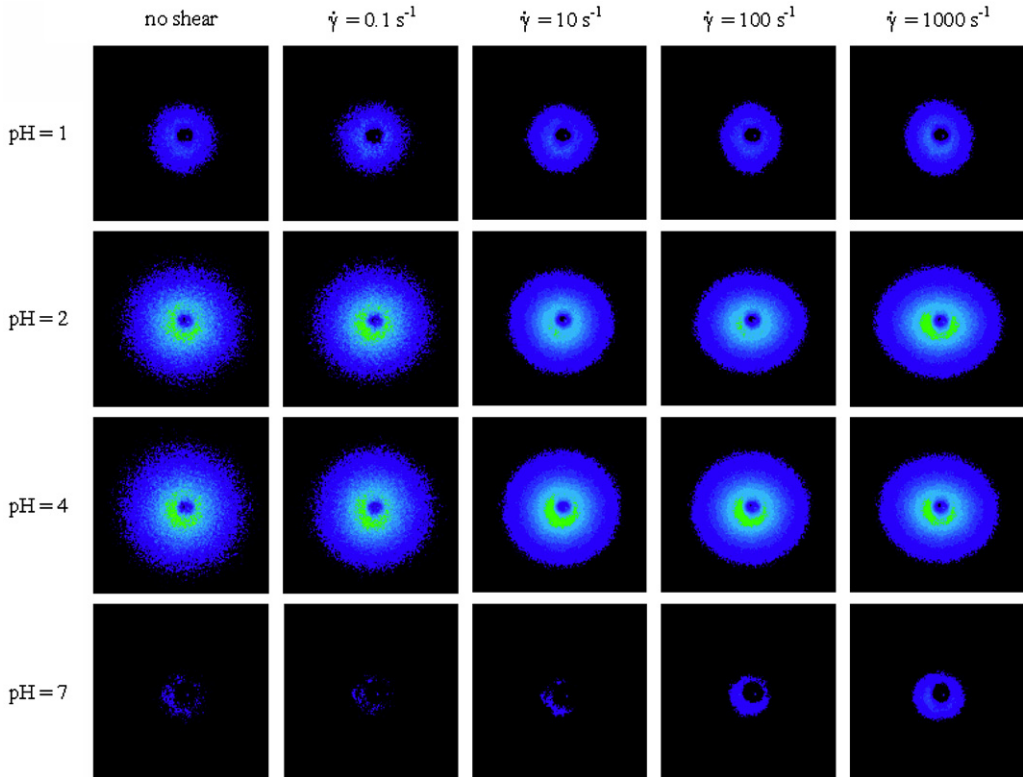

Figure 7. SALS 2 D patterns of 1 wt % solutions of mucin at the pH values indicated and exposed to the stated shear rates.

power law $I(q) \sim q^{-d}$, which yields a good description of the SALS data in the low q region. The values of the power law exponent in the flow direction are given in Figure 10 (the data for the scattering vertically across the flow direction exhibit the same trends). Within experimental errors, the values of the power law exponent are almost independent of the shear rate. It is evident that the values of d are significantly larger ($d \approx 1.9$) at pH 2 and pH 4 than at pH 1 or pH 7 ($d \approx 1.3$). The higher value of d suggests that the association effect is more intensive. Values of d around 2 have frequently been reported[48,50] from SANS experiments on solutions of associating polysaccharides containing hydrophobic moieties. Although enhanced association effects are suggested at pH 2 and 4, the value of d indicates that the system is not close to macroscopic phase separation for which a Porod value[51] of 4 would be expected.[52]

4. Conclusions

In this work the influence of pH on properties of purified pig gastric mucin in aqueous solutions has been examined with the aid of dynamic light scattering, turbidity, and rheo-SALS methods. DLS measurements on dilute solutions of mucin revealed the formation of large association complexes at pH 2, where the polymer has a low charge density or is uncharged. At lower or higher values of pH, the electrostatic repulsive interactions reduce the tendency of the mucin molecules to form interpolymer aggregates. The q dependence of the reduced intensity indicates that the mucin moieties are rather extended at low or high pH, whereas at pH 2 the complexes are rather compact.

In semidilute mucin solutions, the results from DLS show that the relaxation process at all conditions is bimodal, characterized by two stretched exponentials. The fast relaxation mode is always diffusive, and the mesh size determined from the cooperative diffusion coefficient is much higher at pH 2 than at lower or higher pH values. At pH 2, bundles of chains are formed due to hydrophobic interactions and the network is more heterogeneous than at lower or higher pH values, where the polymer chains are more evenly distributed in the network because of repulsive forces. The slow relaxation time is much longer at pH 2 than at the other pH values, demonstrating that the disengagement relaxation of clusters or individual chains is impeded at pH 2 where the coupling of the chains is stronger. Furthermore, both the turbidity and reduced intensity exhibit maximum value at pH 2. The general picture that emerges is that at pH 2 large 'lumps' of polymer are formed and a heterogeneous network with strong connectivity is formed. When the charge density of the polymer is increased, 'lumps' (or junction zones) are gradually

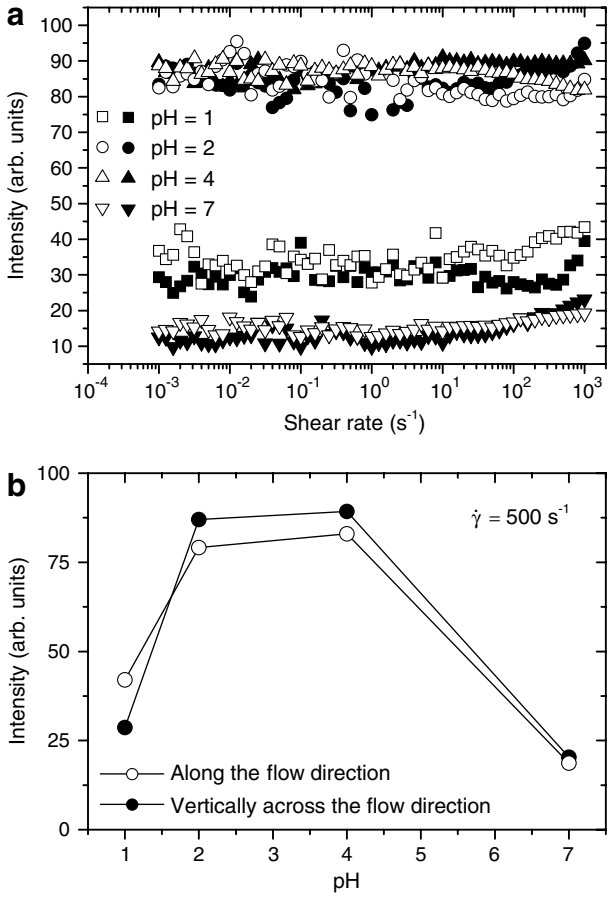

Figure 8. (a) Plot of the scattered intensity ($q = 0.27\ \mu m^{-1}$) versus shear rate for 1 wt % solutions of mucin at the pH values indicated along the flow direction (open symbols) and vertically across (solid symbols). (b) Effect of pH on the scattered intensity at a shear rate of $500\ s^{-1}$ ($q = 0.27\ \mu m^{-1}$) along the flow direction (open symbols) and vertically across (solid symbols).

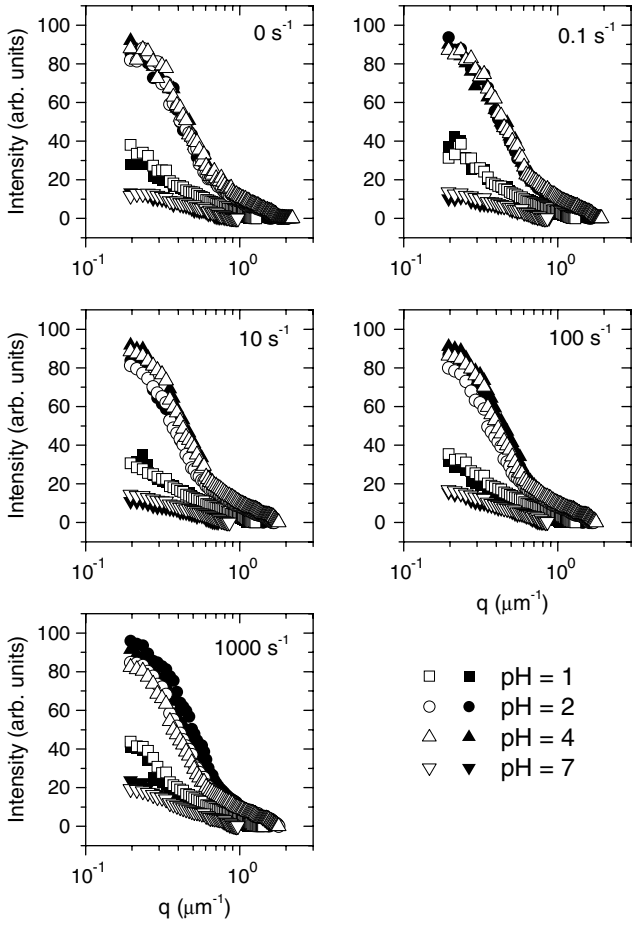

Figure 9. SALS scattered intensity plotted versus scattering vector q (every third point is shown) for 1 wt % solutions of mucin at the pH values and shear rates indicated. The angular dependency of the scattering intensities along the flow direction (open symbols) and vertically across (solid symbols) was analyzed by means of the software program.

disintegrated and a more homogeneous network is evolved with a weaker connectivity.

The rheo-SALS experiments disclose strong shear thinning effects at all pH values, except at pH 1, where Newtonian behavior was found. The viscosity data at a low shear rate passes through a maximum at pH 2, which is similar to that observed for the slow relaxation time from DLS. The low value of τ_s and the Newtonian feature and low viscosity at pH 1 suggest that the network is fragmented with weak connectivity, and is probably composed of chains that are contracted and stabilized by some positive charges bound to the polymer chains. The scattered intensity 2D patterns from SALS are isotropic at low shear rates. At pH 2 and 4, anisotropy in form of elliptical shapes develops at high shear rates. This anisotropy suggests the evolution of enhanced concentration fluctuations at these pH values. The scattered intensity shows at all shear rates a much stronger upturn at low q values for the samples at pH 2 and 4 than at pH 1 or pH 7. This is again an indication

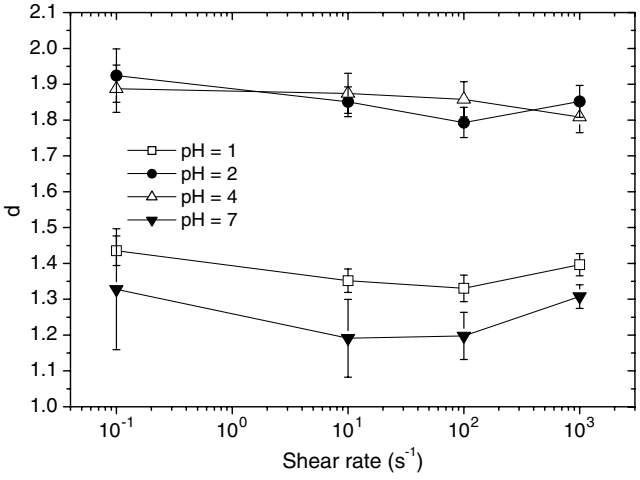

Figure 10. Plot of the power law exponent d ($I(q) \sim q^{-d}$), describing the wave vector dependence of the scattered intensity (in the flow direction), as a function of the shear rate for 1.0 wt % solutions of mucin at the values of pH indicated.

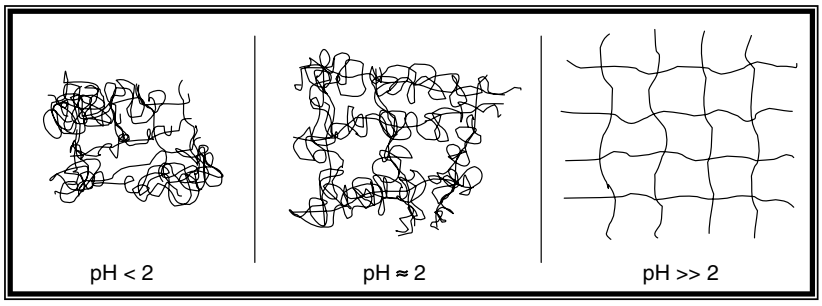

Figure 11. Schematic illustration of the network formation in semidilute mucin solutions at different values of pH.

of that large association structures are formed at pH 2 and pH 4.

A schematic illustration of the network structures at different values of pH is displayed in Figure 11. At pH <2, the contracted chains build up a network with weak connectivity. At pH around 2, a strongly heterogeneous network of intertwined chains is formed, whereas at pH ≫2 the chains are more evenly dispersed and a homogeneous network is evolved.

Acknowledgment

A.M. and B.N. gratefully acknowledge financial support provided by a FUNMAT Project (Novel functional polymer materials for drug delivery applications).

References

1. Allen, A. Structure and Function of Gastrointestinal Mucus. In *Physiology of the Gastrointestinal Tract*; Johnson, L. R., Ed.; Raven Press: New York, 1981; Vol. 1, pp 617–639.
2. Strous, G. J.; Dekker, J. *Crit. Rev. Biochem. Mol. Biol.* **1992**, *27*, 57–92.
3. Bansil, R.; Stanley, H. E.; LaMont, J. T. *Annu. Rev. Physiol.* **1995**, *57*, 635–657.
4. Carlstedt, I.; Sheehan, J. K.; Corfield, A. P.; Gallagher, J. T. *Essays Biochem.* **1985**, *5*, 40–76.
5. Van den Steen, P.; Rudd, P. M.; Dwek, R. A.; Opdenakker, G. *Crit. Rev. Biochem. Mol. Biol.* **1998**, *33*, 151–208.
6. Cao, X.; Bansil, R.; Bhaskar, K. R.; Turner, B. S.; LaMont, J. T.; Niu, N.; Afdahl, N. H. *Biophys. J.* **1999**, *76*, 1250–1258.
7. Waigh, T. A.; Papagiannopoulos, A.; Voice, A.; Bansil, R.; Unwin, A. P.; Dewhurst, C. D.; Turner, B. S.; Afdahl, N. H. *Langmuir* **2002**, *18*, 7188–7195.
8. Longer, M. A.; Robinson, J. R. *Pharm. Int.* **1986**, *7*, 114–117.
9. Hong, Z.; Chasan, B.; Bansil, R.; Turner, B. S.; Bhaskar, K. R.; Afdahl, N. H. *Biomacromolecules* **2005**, *6*, 3458–3466.
10. Bhaskar, K. R.; Gong, D. H.; Bansil, R.; Pajevic, S.; Hamilton, J. A.; Turner, B. S.; LaMont, J. T. *Am. J. Physiol.* **1991**, *261*, 827–832.
11. Lafitte, G.; Söderman, O.; Thuresson, K.; Davies, J. *Biopolymers* **2007**, *86*, 165–175.
12. KocevarNared, J.; Kristl, J.; SmidKorbar, J. *Biomaterials* **1997**, *18*, 677–681.
13. Nordman, H.; Davies, J. R.; Herrmann, A.; Karlsson, N. G.; Hansson, G. C.; Carlstedt, I. *Biochem. J.* **1997**, *326*, 903–910.
14. Siegert, A. J. F. Massachusetts Institute of Technology Rad. Lab. Rep. No. 456, 1943.
15. Bastardo, L.; Claesson, P.; Brown, W. *Langmuir* **2002**, *18*, 3848–3853.
16. Celli, J.; Gregor, B.; Turner, B.; Afdahl, N. H.; Bansil, R.; Erramilli, S. *Biomacromolecules* **2005**, *6*, 1329–1333.
17. Kjøniksen, A.-L.; Nyström, B. *Macromolecules* **1996**, *29*, 7116–7123.
18. Beheshti, N.; Nguyen, G. T. M.; Kjøniksen, A.-L.; Knudsen, K. D.; Nyström, B. *Colloids Surf., A* **2006**, *279*, 40–49.
19. Ngai, K. L. *Adv. Colloid Interface Sci.* **1996**, *64*, 1–43.
20. Shogren, R.; Gerken, T. A.; Jentoft, N. *Biochemistry* **1989**, *28*, 5525–5536.
21. Fefelova, N. A.; Nurkeeva, Z. S.; Mun, G. A.; Khutoryanskiy, V. V. *Int. J. Pharm.* **2007**, *339*, 25–32.
22. Gandhi, R. B.; Robinson, J. R. *Pharm. Res.* **1991**, *8*, 1199–1202.
23. Tur, K. M.; Ch'ng, H.-S. *Int. J. Pharm.* **1998**, *160*, 61–74.
24. Daoud, M.; Martin, J. E. In *The Fractal Approach to Heterogeneous Chemistry*; Avnir, D., Ed.; John Wiley & Sons: New York, 1989.
25. Tirado-Miranda, M.; Schmitt, A.; Callejas-Fernándes, J.; Fernándes-Barbero, A. *Colloids Surf., A* **2000**, *162*, 67–73.
26. Celli, J. P.; Turner, B. S.; Afdhal, N. H.; Ewoldt, R. H.; McKinley, G. H.; Bansil, R.; Erramilli, S. *Biomacromolecules* **2007**, *8*, 1580–1586.
27. Cabane, B.; Lindell, K.; Engström, S.; Lindman, B. *Macromolecules* **1996**, *29*, 3188–3197.
28. Kjøniksen, A.-L.; Nyström, B.; Lindman, B. *Macromolecules* **1998**, *31*, 1852–1858.
29. Tanaka, F. *Adv. Colloid Interface Sci.* **1996**, *63*, 23–40.
30. Semenov, A. N.; Rubinstein, M. *Macromolecules* **1998**, *31*, 1373–1385.
31. Dobrynin, A. V. *Macromolecules* **2004**, *37*, 3881–3893.
32. De Gennes, P.-G. *Scaling Concepts in Polymer Physics*; Cornell University Press: Ithaca, NY, 1979.
33. Martin, J. E.; Wilcoxon, J.; Odinek, J. *J. Phys. Rev. A* **1991**, *43*, 858–872.
34. Ren, S. Z.; Shi, W. F.; Zhang, W. B.; Sorensen, C. M *Phys. Rev. A* **1992**, *45*, 2416–2422.
35. Ren, S. Z.; Sorensen, C. M. *Phys. Rev. Lett.* **1993**, *70*, 1727–1730.
36. Nyström, B.; Walderhaug, H.; Hansen, F. K. *J. Phys. Chem.* **1993**, *97*, 7743–7752.
37. Kjøniksen, A.-L.; Iversen, C.; Nyström, B.; Nakken, T.; Palmgren, O. *Macromolecules* **1998**, *31*, 8142–8148.
38. Hossain, K.; Miyanaga, K.; Maeda, H.; Nemoto, N. *Biomacromolecules* **2001**, *2*, 442–449.

39. Stauffer, D.; Coniglio, A.; Adam, M. *Adv. Polym. Sci.* **1982**, *44*, 103–158.
40. Larson, R. G. *The Structure and Rheology of Complex Fluids*; Oxford University Press: New York, 1999.
41. Helfand, E.; Fredrickson, G. H. *Phys. Rev. Lett.* **1989**, *62*, 2468–2471.
42. Wu, X.-L.; Pine, D. J.; Dixon, P. K. *Phys. Rev. Lett.* **1991**, *66*, 2408–2411.
43. Kadoma, I. A.; van Egmond, J. W. *Langmuir* **1997**, *13*, 4551–4561.
44. Kadoma, I. A.; Ylitalo, C.; van Egmond, J. W. *Rheol. Acta* **1997**, *36*, 1–12.
45. Horkay, F.; Basser, P. J.; Hecht, A.-M.; Geissler, E. *Polym. Prepr. (Am. Chem. Soc., Div. Polym. Chem.)* **2002**, *43*, 369–370.
46. Ermi, B. D.; Amis, E. J. *Macromolecules* **1997**, *30*, 6937–6942.
47. Schmidt, J.; Burchard, W.; Richtering, W. *Biomacromolecules* **2003**, *4*, 453–460.
48. Bu, H.; Kjøniksen, A.-L.; Knudsen, K. D.; Nyström, B. *Langmuir* **2005**, *21*, 10923–10930.
49. Kjøniksen, A.-L.; Knudsen, K. D.; Nyström, B. *Eur. Polym. J.* **2005**, *41*, 1954–1964.
50. Bu, H.; Naess, S. N.; Beheshti, N.; Zhu, K.; Knudsen, K. D.; Kjøniksen, A.-L.; Elgsaeter, A.; Nyström, B. *Langmuir* **2006**, *22*, 9023–9029.
51. Glatter, O.; Kratky, O. *Small Angle X-ray Scattering*; Academic Press: London, 1982.
52. Schubert, B. A.; Wagner, N. J.; Kaler, E. W.; Raghavan, S. R. *Langmuir* **2004**, *20*, 3564–3573.